JACS
JOURNAL OF THE AMERICAN CHEMICAL SOCIETY

Article

pubs.acs.org/JACS

Electrostatic Nucleic Acid Nanoassembly Enables Hybridization Chain Reaction in Living Cells for Ultrasensitive mRNA Imaging

Zhan Wu, Gao-Qin Liu, Xiao-Li Yang, and Jian-Hui Jiang*

State Key Laboratory of Chemeo/Bio-Sensing and Chemometrics, College of Chemistry and Chemical Engineering, Hunan University, Changsha, 410082, P. R. China

Supporting Information

ABSTRACT: Efficient approaches for intracellular delivery of nucleic acid reagents to achieve sensitive detection and regulation of gene and protein expressions are essential for chemistry and biology. We develop a novel electrostatic DNA nanoassembly that, for the first time, realizes hybridization chain reaction (HCR), a target-initiated alternating hybridization reaction between two hairpin probes, for signal amplification in living cells. The DNA nanoassembly has a designed structure with a core gold nanoparticle, a cationic peptide interlayer, and an electrostatically assembled outer layer of fluorophore-labeled hairpin DNA probes. It is shown to have high efficiency for cellular delivery of DNA probes via a unique endocytosis-independent mechanism that confers a significant advantage of overcoming endosomal entrapment. Moreover, electrostatic assembly of DNA probes enables target-initialized release of the probes from the nanoassembly via HCR. This intracellular HCR offers efficient signal amplification and enables ultrasensitive fluorescence activation imaging of mRNA expression with a picomolar detection limit. The results imply that the developed nanoassembly may provide an invaluable platform in low-abundance biomarker discovery and regulation for cell biology and theranostics.

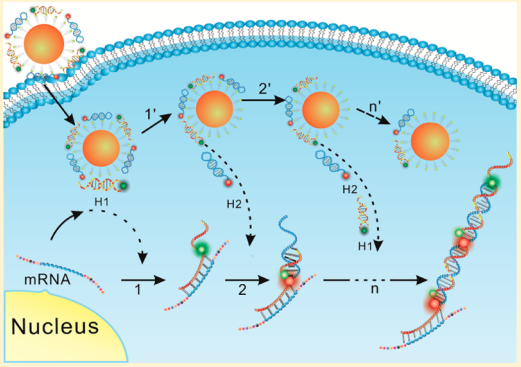

INTRODUCTION

Nucleic acid-based reagents represent an essential tool in detection and regulation of gene expression and protein activity for chemistry and biology.[1] Major challenges of using these nucleic acid reagents for cell biology and theranostics are the efficiency for their delivery into different cells and the sensitivity for target detection and regulation.[2] Recent advance in nanotechnology has fueled the development of nanoscale nucleic acids assemblies for intracellular applications.[3] Notably, spherical nucleic acids (SNA), structures with a template core of inorganic or organic nanoparticles and a shell of oriented nucleic acid reagents, have been extensively explored.[4] These SNA nanostructures are demonstrated to facilitate the internalization of nucleic acid reagents into cells of diverse types,[4a] making them a useful strategy for intracellular detection and gene regulation.[4b,c] Nevertheless, current nucleic acid nanostructures typically exhibit limited sensitivity for intracellular detection and regulation with a detection limit at the nanomolar level.[5] This shortcoming is largely due to the lack of signal amplification mechanisms in these methods. A viable embodiment of signal amplification strategies that are able to be realized in living cells using a specific nucleic acids nanoassembly, therefore, remains an unresolved challenge.

Here we develop a novel electrostatically assembled nucleic acid nanostructure that enables the realization of hybridization chain reaction (HCR)[6] for signal amplification in living cells. A key design to the intracellular signal amplification strategy is a novel nucleic acid nanoassembly with a core gold nanoparticle (AuNP), an interlayer of cysteine-terminated cationic peptides, and an outer layer of fluorophore-labeled nucleic acid probes, as illustrated in Scheme 1. The AuNP core acts as a well-defined template for self-assembly of the cationic peptides, and it also allows efficient quenching for fluorophores labeled at the nucleic acid probes due to surface energy transfer (SET).[7]

Scheme 1. Illustration of the Electrostatically Assembled Nucleic Acid Nanostructure

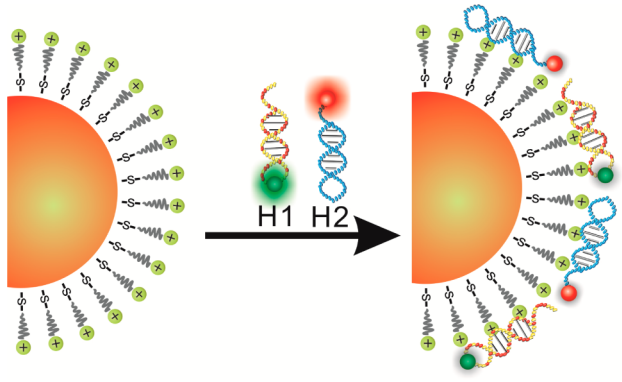

Received: February 17, 2015
Published: May 13, 2015

DOI: 10.1021/jacs.5b01778
J. Am. Chem. Soc. 2015, 137, 6829−6836

Assembly of the peptides CAAAAAAK^{+}(Me)$_3$ via thiol−Au bond generates a compact interlayer through hydrophobic interactions between the six alanine side-chains[8] with cationic terminals exposed on the surface. The cation, a trimethylated lysine residue which is ubiquitous in methylated proteins,[9] is designed to mimic a quaternary ammonium phospholipid phosphatidylcholine and thus expected to have low toxicity. Moreover, it is a pH-independent cationic layer, which confers stable electrostatic assembly for nucleic acid probes in varying acidic or basic biological surroundings.

Unlike classical SNA with oriented nucleic acid probes, the designed nanostructure has a randomly oriented nucleic acid assembly stabilized by synergistic or multiple-site electrostatic interactions between the interlayer and the nucleic acid backbones. Such synergistic interactions typically require a suitable conformation for the probes, implying that target interaction may release these probes away from the particles, as the responsive conformation changes of the probes decrease their affinity. Moreover, dissociation from the particles enables the probes to freely participate in cyclic reactions and ordered assembly, which are essential for nucleic acid amplification.[10] Motivated by this hypothesis, we develop a new HCR-based ultrasensitive signal amplification strategy and in the present study demonstrate its potential for fluorescence activation imaging of mRNA expression in living cells, as shown in Scheme 2. We choose *survivin* mRNA, a mRNA known to be overexpressed in most cancers,[11] as the model target. Two hairpin-structured DNA probes H1 and H2 are designed, one labeled with a fluorescence donor carboxyfluorescein (FAM) and the other labeled with a fluorescence acceptor tetramethylrhodamine (TMR). The loop regions of H1 and H2 are flexible enough to synergistically interact with the cationic surface, enabling H1 and H2 probes to be stably assembled on the peptide-coated particles. This situation gives very weak fluorescence signals for both fluorophores due to efficient quenching by the core AuNPs.[12] The presence of a mRNA target initializes the hybridization with H1 and produces a single stranded tail in H1, which may dissociate or increase the mobility of H1 on the particles, facilitating its hybridization with H2 and restoring a single-strand tail in H2 with the same sequence of target. In this way, a chain reaction is triggered for alternating hybridization between H1 and H2, producing a chain-like assembly of H1 and H2.[6] The HCR product has a rigid duplex conformation, which has decreased affinity to the nanoassembly and thus dissociates from the surface. The dissociated product also draws the fluorescence donors and acceptors into close proximity, activating a Föster resonant energy transfer (FRET) signal indicating target mRNA expression. To our knowledge, this is the first time that efficient intracellular signal amplification has been realized in live cells using a specifically designed nucleic acid nanoassembly. This DNA nanoassembly possesses a unique structure with a cationic interlayer and a gold core, so it offers high efficiency for cellular delivery and fluorescence quenching of the nucleic acid probes. Moreover, the HCR amplification offers very high sensitivity for intracellular detection and thus creates a useful nanosensor platform in low-abundance biomarker discovery and regulation for cell biology and diagnostics.

Scheme 2. Illustration of Intracellular HCR for mRNA Detection[a]

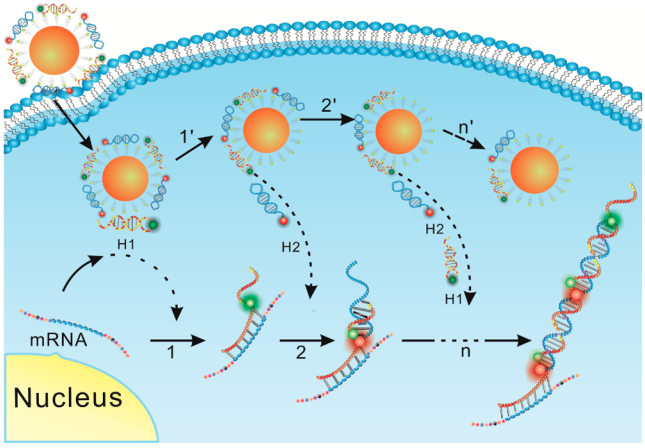

[a]Hybridization of mRNA target with probe H1 on DNA nanoassembly yields a single-strand tail in H1, which then hybridizes with probe H2 and restores a single-strand tail in H2 with the same sequence of target. In this way a chain reaction of alternating hybridization between H1 and H2 was triggered, producing a chain-like duplex assembly of H1 and H2 that dissociates from the nanoassembly and activates a FRET signal.

RESULTS AND DISCUSSION

Synthesis and Characterization of DNA Nanoassembly. The electrostatically assembled DNA nanostructure was readily synthesized using a two-step self-assembly procedure using cetyltrimethylammonium bromide (CTAB) stabilized AuNPs as the starting material. First, the peptide-coated AuNPs were prepared via ligand exchange by incubating the cysteine-terminated peptides with CTAB-stabilized AuNPs. Then, the nucleic acid nanoassembly was directly obtained by incubating peptide-coated AuNPs with two hairpin DNA probes H1 and H2. This two-step self-assembly procedure allows a rapid (~4 h) synthesis of the nucleic acid nanostructure. Moreover, the as-prepared nanoassembly was found to be dispersed very stably in human serum and high salt (0.5 M NaCl) solutions (Figure S1 in Supporting Information), indicating the possibility of using this nanoassembly in complicated biological systems.

The synthesis of the nanoassembly was characterized by transmission electron microscope (TEM) using negative staining (Figure 1 and Figure S2 in Supporting Information). After displacement of CTAB by the cationic peptides, the nanoassembly showed a very thin peptide coating (~3 nm) on the gold core (~16 nm). The thickness of the peptide layer was close to the contour length (~3.4 nm) for the peptide (0.38 nm per animo acid).[13] After electrostatic assembly of the DNA probes, the nanoassembly gave a typical image for a core−shell structure with a shell thickness ~6 nm. Dynamic light scattering (DLS) analysis showed stepwise increases of the average hydrodynamic diameters from ~17 to ~24 nm and up to ~65 nm during the two-step assembly processes. Zeta potential measurements revealed remarkable alterations of surface charges during the synthesis and manifested a highly negatively charged surface for the DNA nanoassembly. These results gave clear evidence for the successful two-step self-assembly synthesis of the nanoassembly. The loadings of the cationic peptides and the DNA probes on AuNPs were estimated to be ~796 ± 26 molecules and ~42 ± 5 molecules per particle, respectively, via decomposition of the AuNP cores using KCN.[14] The loading of peptides was consistent with those

DOI: 10.1021/jacs.5b01778
J. Am. Chem. Soc. 2015, 137, 6829−6836

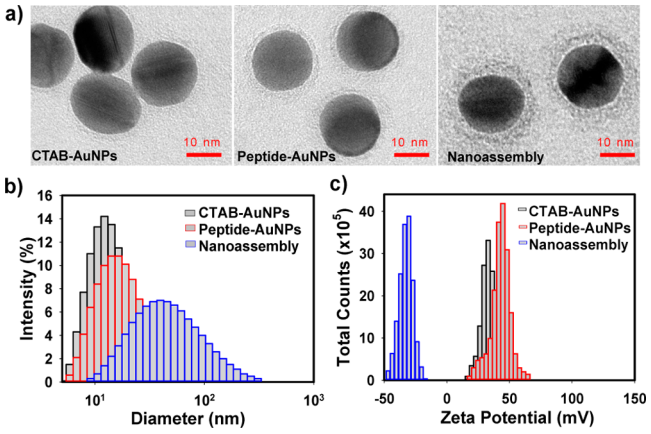

Figure 1. (a) TEM images, (b) DLS analysis, (c) zeta potential analysis for CTAB-coated AuNPs, peptide-coated AuNPs, and DNA nanoassembly.

previously reported for peptide-modified AuNPs,[15] indicators of a compactly packed peptide interlayer that was ascribed to the hydrophobic side-chain interactions.[8] The loading of DNA probes was slightly lower but in the same order of magnitude for SNA,[16] suggesting the capacity of the electrostatic assembled DNA nanostructure for high-loading intracellular delivery of nucleic acid reagents. Moreover, the nanoassembly displayed a weak fluorescence signal in the wavelength range of 500−600 nm with estimated fluorescence quenching efficiencies of ∼94% and 91%, respectively, for FAM and TMR (Figure S3 in Supporting Information). According to the SET model,[17] the distance from the AuNP surface to the FAM labeling site (stem region of the hairpin probe) was calculated to be ∼3.6 nm. Such a small distance suggested that electrostatic assembly was stable enough to retain the DNA probes in a lying-down conformation on the cationic surface.

***In Vitro* Response of DNA Nanoassembly.** Because of the FRET-based design and the activation of both of the fluorescence donor and acceptor, the HCR-based nanosensor strategy showed a particular fluorescence response for *in vitro* detection of a synthetic RNA target (Figure 2a). The nanoassembly merely displayed very weak fluorescence at both emission peaks of FAM and TMR, validating the high

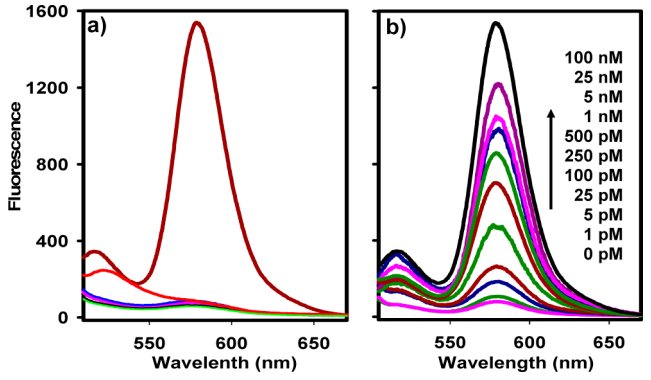

Figure 2. (a) Fluorescence spectral responses obtained by incubating nanoassembly carrying H1 and H2 with target RNA (brown), 10% bovine serum (red), C166 cell lysate (blue), nonhomologous RNA (green), and assay buffer (pink) as well as incubating nanoassembly carrying H3 and H4 with target RNA (black). (b) Fluorescence spectral responses to RNA target of varying concentrations.

quenching efficiencies for these fluorophores by AuNPs. In the presence of 100 nM target RNA, an intense peak was obtained at 582 nm on excitation at 488 nm, indicating an efficient FRET from FAM to TMR. The fluorescence peak for FAM also exhibited a substantial increase, which was attributed to the fact that in the HCR product TMR showed lower quenching efficiency for FAM, while in the nanoassembly AuNPs had higher quenching efficiency for FAM. The peak for TMR gave a very high signal-to-background ratio of ∼13.9-fold in response to 100 nM RNA target, while the peak for FAM showed a relatively smaller signal-to-background ratio of ∼4.5-fold. In contrast, no appreciable fluorescence enhancement appeared in response to a nonhomologous RNA (a synthetic RNA with the most similar sequence to target RNA in human transcripts).[18] A control experiment with a nanoassembly carrying two different hairpin probes H3 and H4 also did not give an activated fluorescence response to target RNA. These results testified that the nanosensor strategy was selective to the HCR reaction between target RNA and its specific hairpin probes. On the other hand, the nanosensor was found to only display marginal fluorescence activation when incubated with a lysate for C166 cells, which had no expression of target mRNA.[19] This finding manifested that the nanosensor was able to offer high selectivity for target RNA detection in cells. In a cell growth medium containing 10% bovine serum, we observed that the near-excitation region (<575 nm) showed an appreciable fluorescence increase, but the FRET signal obtained at the emission peak of TMR (582 nm) did not display remarkable fluorescence activation. Such a fluorescence response was ascribed to the autofluorescence background of the serum matrix. This result revealed that, by taking advantage of the long Stokes shift for the FRET signal, we were able to eliminate the interferences from autofluorescence of biological matrices.

Gel electrophoresis analysis revealed that many bright bands with a maximum size over 5000 base-pairs were obtained for incubating target RNA with two DNA probes H1 and H2 or with the nanoassembly carrying both H1 and H2 (Figure S4 in Supporting Information). These bands evidenced the formation of chain-like duplex assemblies consisting of hundreds of H1 and H2, indicating the potential of the HCR reactions for >100-fold signal amplification in target detection. A control experiment using nonhomologous RNA did not yield a band with large molecular weight. These results evidenced the success of HCR between the nanoassembly and target RNA and verified its specificity. In addition, we found that no bright bands were obtained for the nanoassembly solution unless it was incubated target RNA. This finding verified the stable adsorption of DNA probes on the particle surface and the dissociation of HCR products away from the nanoassembly, which gave a clear evidence for the response mechanism of HCR-based nanosensor strategy.

A close inspection was performed using nanoassembly merely carrying probe L1, a linear and truncated version of H1 (Figure S5 in Supporting Information). Incubation of this L1-carrying nanoassembly with 100 nM RNA target gave a strong fluorescence peak, indicating the dissociation of probe L1 after it formed a duplex with target RNA. This finding manifested that duplex conformation had decreased affinity and tended to dissociate from the nanoassembly. Further experiment by incubating 1 nM RNA target with the L1-carrying nanoassembly showed much smaller fluorescence signal than that obtained with the nanoassembly carrying H1 and H2. These data confirmed efficient signal amplification for our

DOI: 10.1021/jacs.5b01778
J. Am. Chem. Soc. 2015, 137, 6829−6836

nanoassembly-based HCR method. Other experiments by using nanoassembly merely carrying H1 or H2 revealed that hybridization of RNA target with H1 could cause dissociation of H1 from the surface but had no effect on H2 on the nanoassembly. The dissociation of H1 was also attributed to the formation of a duplex conformation with target RNA. This result gave clear evidence for the dissociation of the HCR product from the nanoassembly, verifying the fluorescence activation mechanism for our nanoassembly-based HCR method.

The nanosensor showed fluorescence activation signals dynamically correlated to the concentrations of target RNA through a five-decade range from 1 pM to 100 nM (Figure 2b). A quasi-linear correlation was obtained for the peak intensities at 582 nm to the target RNA concentrations (logarithmic scale) in the range from 1 pM to 1 nM with an estimated detection limit as low as 0.5 pM (Figure S6 in Supporting Information). Assuming a typical diameter of ~10 μm for human cells,[20] such a detection limit actually meant <1 molecule in a cell. This result suggested that the developed nanosensor held the potential for highly sensitive analysis, which might realize detection of a single molecule in a single cell.

In addition, we found that the nanoassembly-based HCR strategy gave much faster kinetics than the standard HCR (Figure S7 in Supporting Information), indicating an improved speed for the developed assay. Presumably, such a faster kinetics was ascribed to possible adsorption of the intermediate product on the nanoparticle surface through its single-strand tail, which might facilitate its hybridization with probes adsorbed on the same particle and thus accelerate the chain reaction.

To apply the nanosensor strategy for mRNA detection in live cells, the toxicity of the nanoassembly and the stability of DNA probes against nuclease were major concerns. It was observed that the nanoassembly only exhibited marginal toxicity to HeLa cells at a concentration up to 200 μg mL^{-1} with the cell viability decreased by ~7% after 8 h incubation (Figure S8 in Supporting Information). These data demonstrated the excellent biocompatibility for the nanoassembly. Interestingly, a thiolated quaternary ammonium compound was previously reported for modification of gold nanorods with low toxicity and efficient cell uptake.[21] Our design of using trimethylated peptides for AuNPs' modification might create a more low-toxic and simple strategy because of its biological origin and common availability from solid synthesis.

The designed DNA nanoassembly was also found to exhibit resistance to degradation by nuclease such as DNase I (Figure S9 in Supporting Information). Actually, there was no substantial degradation for the DNA nanoassembly when incubated with DNase I, and the initial degradation rate was more than 10-fold slower than that for the corresponding DNA probe. This improved nuclease resistance was attributed to the too high steric hindrance for nuclease to interact the DNA, which indicated a high-affinity electrostatic assembly of the probes on the cationic surface. The enzyme−substrate association constants K_m were calculated to be 1.4 and 14.8 μM^{-1}, respectively, while the maximum reaction velocity V_{max} were 0.45 and 0.04 nM s^{-1}, respectively, for the DNA probe and the nanoassembly. These data implied that the improved nuclease resistance originated from the remarkably decreased enzyme-binding constant and hydrolysis rate for the nanoassembly.[22] The findings of biocompatibility and nuclease resistance of the nanoassembly, therefore, supported its potential for biomedical applications.

Cellular Uptake and Localization of DNA Nanoassembly. Further investigation of cellular uptake of the nanoassembly in HeLa cells was performed using dark-field resonant light scattering imaging (Figure S10 in Supporting Information). The dark-field microscopy image showed a crowd of bright spots with typical cytosolic localization when cells incubated with the nanoassembly at 37 °C for 1 h. These bright spots were ascribed to the nanoassembly or its aggregates,[23] evidencing rapid and efficient internalization of the nanoassembly into the cells. Surprisingly, for cells incubated with the nanoassembly for 1 h at 4 °C, we also observed lots of bright spots in the dark-field image. This temperature-independent internalization suggested that intracellular uptake of the nanoassembly did not involve the endocytic pathway.[24] Another experiment by pretreating the cells with NaN_3, an inhibitor for ATPase involved in all energy-dependent endocytic pathways,[25] also showed no reduced uptake for the nanoassembly. This finding gave additional evidence that cellular internalization process of the nanoassembly was independent of normal endocytosis.

A further experiment using single-particle ICP-MS detection[26] revealed that there was no substantial difference in the concentrations for AuNPs in the cells, regardless of the incubation temperatures of 37 or 4 °C or the pretreatment with NaN_3 (Figure S11 in Supporting Information). These data confirmed that the nanoassembly transported across the plasma membrane without being endocytosed. This endocytosis-independent mechanism was very attractive, because it conferred an advantage over routine nanoparticle delivery systems in overcoming insufficient endosomal escape and subsequent lysosomal degradation. To our knowledge, similar cellular internalization behavior had been merely described for cell penetrating peptides, but very rarely reported for nanoparticles.[27] In addition, the concentrations for AuNPs in these cells were estimate to be ~4.2 × 10^5 particles per cell. Such a high cytosolic concentration suggested a high internalization efficiency of the nanoassembly in living cells, implying its potential for live cell detection and theranostics. Furthermore, TEM imaging of microtomed cross sections (~75 nm thickness) of the cells was performed to show a more precise localization of the nanoassembly (Figure S12 in Supporting Information). It was observed that most of nanoparticles were localized outside the lysosomes in the cell cross sections, which were consistent with the endocytosis-independent mechanism for cellular uptake of the nanoassembly.

Live Cell Imaging of mRNA with DNA Nanoassembly. The *in vitro* response and efficient cytosolic delivery of the nanoassembly provided us the possibility for ultrasensitive imaging of mRNA expression in living cells (Figure 3). When HeLa cells incubated with the nanoassembly carrying probes H1 and H2, we obtained very bright and faint fluorescence images, respectively, at the orange (575−610 nm) and the green (510−550 nm) channels with clear cytosolic localization under the excitation at 488 nm. The activation of an intense FRET signal at the orange channel suggested the formation of chain-like assemblies of H1 and H2, a direct evidence for the successful realization of HCR and the expression of target mRNA in the cells. The weak green image was attributed to slightly enhanced fluorescence for the FAM labels, because in the HCR product TMR showed lower quenching efficiency for

DOI: 10.1021/jacs.5b01778
J. Am. Chem. Soc. 2015, 137, 6829−6836

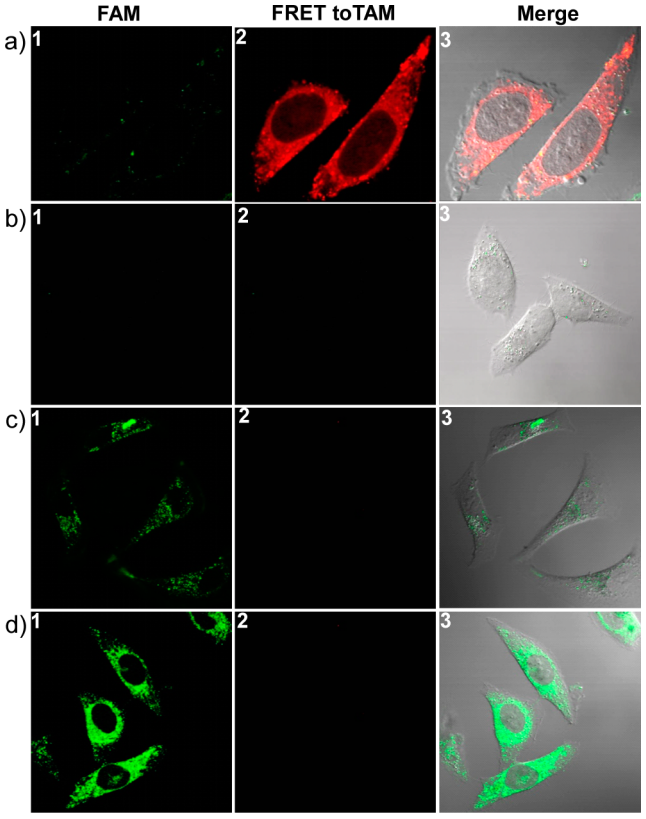

Figure 3. Fluorescence images for cells. (a) HeLa cells incubated with nanoassembly carrying H1 and H2, (b) C166 cells incubated with nanoassembly carrying H1 and H2, (c) HeLa cells incubated with nanoassembly carrying L1, and (d) HeLa cells incubated with nanoassembly carrying H1 and H5.

FAM, while in the nanoassembly AuNPs had higher quenching efficiency for FAM. A control experiment using C166 cells with no expression of target mRNA[19] revealed that there was no fluorescence activation after incubation with the nanoassembly carrying probes H1 and H2. This observation manifested the specificity of the HCR-based strategy for target mRNA imaging. On the other hand, incubation of HeLa cells with a nanoassembly merely carrying probe L1, a linear and truncated version of H1, gave a low-contrast green fluorescence image. Note that L1 formed a duplex conformation with target mRNA and gave a response correlated to target concentration. Thus, this result indeed indicated a much lower fluorescence signal in the absence of HCR amplification. To provide direct evidence for sensitivity enhancement of the HCR-based strategy, we then performed an additional experiment by incubating HeLa cells with a nanoassembly carrying probe H1 as well as H5, a nonlabeled version of H2. As anticipated, we achieved a very bright fluorescence image at the green channel, which was much more intense than that obtained only with probe L1. This finding verified substantial sensitivity enhancement for the developed HCR-based strategy for live cell imaging. Further inspection using flow cytometry also confirmed that the HCR-based strategy offered remarkable enhancement in sensitivity for fluorescence detection of living cells (Figure S13 in Supporting Information). In addition, further control experiments using nanoassembly merely carrying H1 showed a low-contrast green image, indicating possible dissociation of the hybridization product between H1 and target mRNA. No fluorescence signal was obtained for cells incubated with nanoassembly merely carrying H2. These results gave further evidence for the specificity of the FRET signal to HCR reaction (Figure S14 in Supporting Information). A colocalization study of the fluorescence signals revealed that the HCR product exhibited typically cytosolic localization outside the lysosomes, further verifying the endocytosis-independent mechanism for cellular uptake of the nanoassembly (Figure S15 in Supporting Information). An additional gel electrophoresis analysis showed that HCR products with large molecule weights were obtained from cytoplasm extracts of the cells incubated with nanoassembly carrying H1 and H2. This finding confirmed the successful realization of HCR in living cells using the nanoassembly, implying its potential for efficient signal amplification (Figure S16 in Supporting Information).

Next, the potential of the developed strategy for quantitative evaluation of the mRNA expression in living cells was explored. It was found that, after HeLa cells treated with increasing concentrations of YM155, an imidazolium-based compound specifically repressing *survivin* mRNA expression,[28] the cells displayed fluorescence images with decreased brightness (Figure 4). This result suggested that YM155 was a potent

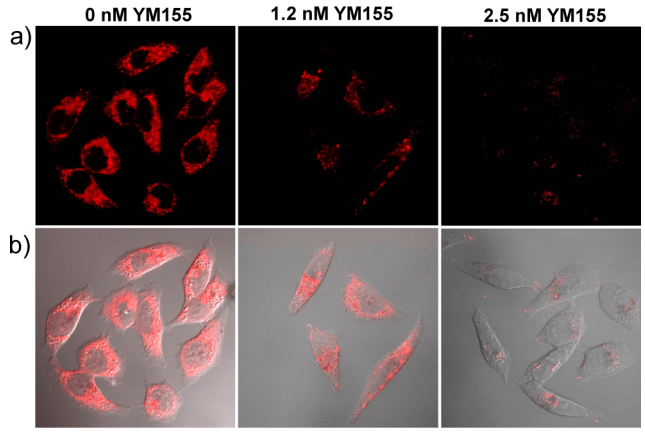

Figure 4. Fluorescence images for Hela cells treated with varying concentrations of a *survivin* expression repressor YM155 followed by incubation with the nanoassembly. (a) Orange fluorescence, (b) merged fluorescence, and differential interference contrast image.

suppressant for *survivin* mRNA expression, and the mRNA was down-regulated significantly in a manner dependent upon the dose of YM155. A further analysis for quantification of the intracellular mRNA using a large pool of cells was performed by fluorescence imaging, flow cytometry, and real-time reverse transcription polymerase chain reaction (RT-PCR) (Figures S17−S19 in Supporting Information). The results revealed that the developed strategy was able to give fluorescence signals dynamically correlated to the expression level of target mRNA, confirming that this strategy had the potential for quantifying mRNA expression in living cells.

On the other hand, the relative expression levels of the mRNA in different cell lines, MCF-10A, MCF-7, and SKBR-3 cells, were also determined using the developed strategy (Figure 5). We obtained fluorescence images of varying brightness in different cells, and SKBR-3 cells showed the highest expression of *survivin* mRNA, while MCF-10 had the lowest expression. This result was consistent with previous report for the relative expression levels of *survivin* mRNA.[29] Moreover, the images showed fluorescence brightness dynamically correlated to the relative concentrations of target mRNA

DOI: 10.1021/jacs.5b01778
J. Am. Chem. Soc. 2015, 137, 6829−6836

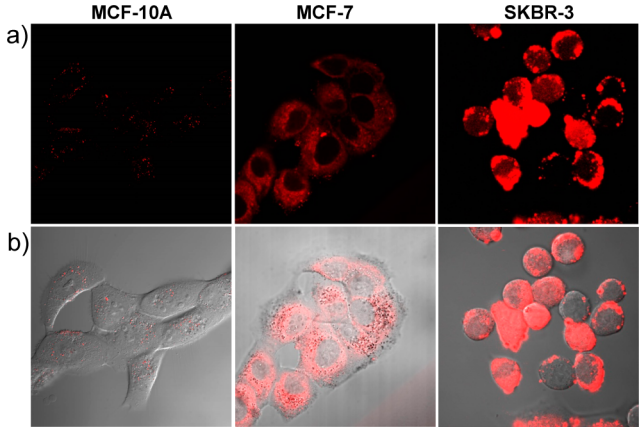

Figure 5. Fluorescence images for different cells incubated with the nanoassembly. (a) Orange fluorescence, (b) merged fluorescence, and differential interference contrast image.

in these cells analyzed by RT-PCR (Figure S20 in Supporting Information). Such concentration-dependent fluorescence image responses to target mRNA implies the potential of the HCR-based strategy for quantitative imaging of target mRNA in living cells.

CONCLUSION

We have developed a novel electrostatically assembled nucleic acid nanostructure that, for the first time, realizes HCR in living cells. This intracellular HCR strategy creates enormous signal amplification and, thus, enables ultrasensitive fluorescence activation imaging of mRNA expression with a detection limit close to single molecule per cell. This specifically designed nucleic acid nanoassembly can be prepared easily and rapidly through a two-step assembly process. It is demonstrated to exhibit excellent biocompatibility and high resistance to DNase-mediated degradation. Because of its unique structure with a cationic peptide interlayer and electrostatically assembled DNA shell, the nucleic acid nanoassembly offers high efficiency for cellular delivery and fluorescence quenching of the nucleic acid probes. It is shown to facilitate highly efficient cellular delivery of DNA probes via a unique endocytosis-independent mechanism that confers an advantage in overcoming endosomal entrapment. Moreover, live cell assays reveal that the developed strategy is very selective to target mRNA and has the potential for quantitative imaging of mRNA expression. In virtue of these advantages, the nanoassembly might provide an invaluable platform in low-abundance biomarker discovery and regulation for cell biology and theranostics.

EXPERIMENTAL SECTION

Materials. Hydrogen tetrachloroaurate (III) ($HAuCl_4 \cdot 4H_2O$, 99.99%), sodium azide (NaN_3), hexadecyltrimethylammonium bromide (CTAB), phosphotungstic acid, and *survivin* expression repressor YM155 were purchased from Sigma-Aldrich (St. Louis, USA). HeLa cells (human cervical carcinoma cell line) and C166 cells (mouse endothelial cell line) were obtained from the cell bank of Central Laboratory at Xiangya Hospital (Changsha, China). MCF-7 (human breast adenocarcinoma cell line), MCF-10A cells (immortalized nontumorigenic human mammary epithelial cell line), and SKBR-3 cells (human breast cancer cell line) were purchased from Cell Bank of the Committee on Type Culture Collection of Chinese Academy of Sciences (Beijing, China). Cell culture media was obtained from Thermo Scientific HyClone (MA, USA). CellTiter96 AQueous One Solution Cell Proliferation Assay kit was purchased from Promega (Madison, WI). TRAPeze 1× CHAPS Lysis Buffer was purchased from Millipore (Billerica, MA). All other chemicals were of analytical grade and obtained from Sinopharm Chemical Reagent Co. Ltd. (Shanghai, China). All solutions were prepared uBillerica, MA) with an electric resistance >18.3 MΩ. The peptide $CAAAAAAAK(ME)_3$ (N-to-C direction) with C-terminal amidation was chemically synthesized by a solid-phase method from China Scilight Biotechnology Co. (95% purity). Oligonucleotides used in this work were synthesized from Takara Biotechnology Co. Ltd. (Dalian, China). Thermodynamic parameters of oligonucleotides were calculated using bioinformatics software (http://www.bioinfo.rpi.edu/applications/). Sequences of the synthesized oligonucleotides are given in Supporting Information Table S1.

Synthesis of DNA Nanoassembly. The peptide-modified AuNP was prepared by adding dropwise 30 μL of 1 mM peptide solution in 2.5 mL of 3 nM CTAB-stabilized AuNPs (~17 nm). The resulting mixture was gently stirred for 3 h followed by centrifuging twice at 15,000 rpm for 10 min to remove excessive unbound peptide. The sediments were redispersed in 2.5 mL sterile ultrapure water. The final concentration of peptide-modified AuNPs was estimated to be ~3 nM, assuming that there was only a negligible loss during the peptide modification processes.

The DNA nanoassembly was prepared by mixing 25 μL of 10 μM probe H1 and 25 μL 10 μM probe H2 solution with 1 mL of 3 nM peptide-modified AuNPs followed by vortex agitating at room temperature for 30 min. The mixture was centrifuged twice at 15,000 rpm for 10 min to remove excessive DNA probes. The nanoassembly sediments were resuspended in 1 mL phosphate buffer saline (PBS, pH 7.4) containing 10 mM phosphate, 2.7 mM KCl, 137 mM NaCl, and 5 mM $MgCl_2$. The final concentration of DNA nanoassembly was estimated to be ~9 nM, assuming that there was only a negligible loss during the synthesis.

***in Vitro* Detection of RNA Target.** In 100 μL of 3 nM nanoassembly solution, 20 μL sample of a given concentration of target RNA was added followed by incubation at 37 °C for 3 h. The resulting mixture was immediately subjected to fluorescence measurements. Fluorescence spectra were recorded using an F-7000 spectrofluorometer (Hitachi, Japan) with excitation at 488 nm. The slit was set to be 5 nm for both the excitation and the emission.

The control bovine serum sample was obtained by diluting fetal bovine serum by 10-fold with PBS. The control cell lysate sample was obtained by mixing 10^5 C166 cells with TRAPeze 1× CHAPS Lysis Buffer, followed by incubation on ice for 30 min and collection of the supernatant after centrifuging at 14,000 *g* for 10 min at 4 °C.

Cell Culture and Optical Imaging. HeLa cells and MCF-7 cells were cultured in RPMI 1640 medium supplemented with 10% fetal bovine serum, 100 U mL^{-1} penicillin, and 100 U mL^{-1} streptomycin. MCF-10A cells were grown in Dulbecco's-modified Eagles medium (DMEM) containing 100 ng mL^{-1} cholera toxin supplemented with 10% fetal bovine serum, 100 U mL^{-1} penicillin, and 100 U mL^{-1} streptomycin. SKBR-3 cells were grown in McCoy's 5A medium (modified with tricine) supplemented with 10% heat-inactivated fetal bovine serum. C166 cells were incubated in DMEM supplemented with 10% fetal bovine serum. All cell lines were maintained at 37 °C in a 100% humidified atmosphere containing 5% CO_2. The cell density was determined using a TC20 automated cell counter (BIO-RAD, USA).

Fluorescence imaging of cells was performed as follows: Cells were plated on a 35 mm Petri dish with 10 mm well in 2 mL culture medium at 37 °C for 24 h, then incubated with 1 mL culture medium containing 0.3 nM nanoassembly at 37 °C for 3 h. After washing three times with cold PBS, the cells were incubated with 1 mL fresh medium at 37 °C before imaging. The experiments in which *survivin* mRNA expression was downregulated were performed as follows: HeLa cells, plated on a 35 mm Petri dish after 24 h incubation, were first pretreated at 37 °C for 48 h with 1 mL culture medium containing YM155 of a given concentration. Then, the cells were washed and incubated with 1 mL culture medium containing 0.3 nM nanoassembly at 37 °C for 3 h followed by incubation with 1 mL fresh medium at 37 °C before imaging.

DOI: 10.1021/jacs.5b01778
J. Am. Chem. Soc. 2015, 137, 6829−6836

Fluorescence imaging of intracellular localization for the nanoassembly was performed as follows: Cells plated on a 35 mm Petri dish were incubated with 1 mL culture medium containing 0.3 nM nanoassembly at 37 °C for 3 h. After washing three times with cold PBS, the cells were incubated with fresh RPMI 1640 medium containing 25 nM Lysosome traker (Lyso@tracker green) for 15 min followed by imaging.

Dark-field microscopy image for cellular uptake of DNA nanoassembly was performed as follows: Cells were grown on glass coverslips placed at the bottom of 6-well tissue culture plates at 37 °C for 24 h and then incubated with 1 mL culture medium containing 0.3 nM nanoassembly at 37 °C for 1 h. The coverslips were taken out and washed three times with cold PBS before imaging. For cellular uptake experiment at 4 °C, cells grown on glass coverslips were first incubated at 4 °C for 0.5 h and then grown in 1 mL culture medium containing 0.3 nM nanoassembly at 4 °C for 1 h followed by imaging. For cellular uptake experiment in the presence of NaN_3, cells grown on glass coverslips were first pretreated at 37 °C for 1 h with 1 mL culture medium containing 1% NaN_3 and then incubated with 1 mL culture medium containing 0.3 nM nanoassembly and 1% NaN_3 at 37 °C for 1 h followed by imaging.

All fluorescence images were acquired using an oil dipping objective (100× , 1.25 NA) on a confocal laser scanning fluorescence microscope setup consisting of an Olympus LX 81 inverted microscope with an Olympus FV1000 confocal scanning system. A 488 nm laser was used as the excitation source, and emission was collected using a 100 μm pinhole at two separate channels, green (510−550 nm) and red (575−610 nm).

Dark-field microscopy images were acquired on an upright optical microscope Nikon 80i (Japan). White light from the halogen lamp was focused onto the sample obliquely via an oil immersion dark-field condenser (NA 1.43−1.20). Scattered light from the nanoassembly was collected using a 60× objective and then captured using a color CCD camera (DP72, Olympus).

■ ASSOCIATED CONTENT

Ⓢ Supporting Information

Additional experimental details and figures. The Supporting Information is available free of charge on the ACS Publications website at DOI: 10.1021/jacs.5b01778.

■ AUTHOR INFORMATION

Corresponding Author

*jianhuijiang@hnu.edu.cn

Notes

The authors declare no competing financial interest.

■ ACKNOWLEDGMENTS

This work was supported by NSFC (21190041, 20140540, 201307029, 21205034, 21221003) and National Key Basic Research Program (2011CB911000).

■ REFERENCES

(1) (a) Breaker, R. R. *Nature* **2004**, *432*, 838−845. (b) Vinkenborg, J. L.; Karnowski, N.; Famulok, M. *Nat. Chem. Biol.* **2011**, *7*, 519−527. (c) Wiedenheft, B.; Sternberg, S. H.; Doudna, J. A. *Nature* **2012**, *482*, 313−338. (c) Castel, S. E.; Martienssen, R. A. *Nat. Rev. Genet.* **2013**, *14*, 100−112.

(2) (a) Kanasty, R.; Dorkin, J. R.; Vegas, A.; Anderson, D. *Nat. Mater.* **2013**, *12*, 967−977. (b) Yin, H.; Kanasty, R. L.; Eltoukhy, A. A.; Vegas, A. J.; Dorkin, J. R.; Anderson, D. G. *Nat. Rev. Genet.* **2104**, *15*, 541−555.

(3) (a) Luo, D.; Saltzman, W. M. *Nat. Biotechnol.* **2000**, *18*, 33−37. (b) Sokolova, V.; Epple, M. *Angew. Chem., Int. Ed.* **2008**, *47*, 1382−1395. (c) Chou, L. Y.; Zagorovsky, K.; Chan, W. C. *Nat. Nanotechnol.* **2014**, *9*, 148−155. (d) Li, L. L.; Wu, P.; Hwang, K.; Lu, Y. *J. Am. Chem. Soc.* **2013**, *135*, 2411−2414. (e) Cheng, T. T.; Tian, X.; Liu, C.-L.; Ge, J.; Chu, X.; Li, Y. *J. Am. Chem. Soc.* **2015**, *137*, 982−989.

(4) (a) Rosi, N. L.; Giljohann, D. A.; Thaxton, C. S.; Lytton-Jean, A. K. R.; Han, M. S.; Mirkin, C. A. *Science* **2006**, *312*, 313−338. (b) Cutler, J. I.; Auyeung, E.; Mirkin, C. A. *J. Am. Chem. Soc.* **2012**, *134*, 1376−1391. (c) Zheng, D.; Giljohann, D. A.; Chem, D. L.; Massich, M. D.; Wang, X. Q.; Iordanov, H.; Mirkin, C. A.; Paller, A. S. *Proc. Natl. Acad. Sci. U.S.A.* **2012**, *109*, 11975−11980.

(5) (a) Jayagopal, A.; Halfpenny, K. C.; Petez, J. W.; Wright, D. W. *J. Am. Chem. Soc.* **2010**, *132*, 9789−9796. (b) Prigodich, A. E.; Randeria, P. S.; Briley, W. E.; Kim, W. L.; Daniel, W. L.; Giljohann, D. A.; Mirkin, C. A. *Anal. Chem.* **2012**, *84*, 2062−2066. (c) Li, N.; Chang, C.; Pan, W.; Tang, B. *Angew, Chem. Int. Ed.* **2012**, *51*, 7426−7430.

(6) (a) Dirks, R. M.; Pierce, N. A. *Proc. Natl. Acad. Sci. U.S.A.* **2004**, *101*, 15275−15278. (b) Choi, H. M.; Chang, J. Y.; Trinh, L. A.; Padilla, J. E.; Fraser, S. E.; Pierce, N. A. *Nat. Biotechnol.* **2010**, *28*, 1208−1212. (c) Huang, J.; Wu, Y.; Chen, Y.; Zhu, Z.; Yang, X.; Yang, C. J.; Wang, K.; Tan, W. *Angew. Chem., Int. Ed.* **2011**, *50*, 401−404. (d) Li, F.; Zhang, H.; Wang, Z.; Li, X.; Li, X. F.; Le, X. C. *J. Am. Chem. Soc.* **2013**, *135*, 2443−2446. (e) Jung, C.; Ellington, A. D. *Acc. Chem. Res.* **2014**, *47*, 1825−1835.

(7) (a) Jennings, T. L.; Singh, M. P.; Strouse, G. F. *J. Am. Chem. Soc.* **2006**, *128*, 5462−5467. (b) Wang, F.; Wang, J.; Liu, X. *Angew. Chem., Int. Ed.* **2010**, *49*, 7456−7460.

(8) (a) Silva, G. A.; Czeisler, C.; Niece, K. L.; Beniash, E.; Harrington, D. A.; Kessler, J. A.; Stupp, S. I. *Science* **2004**, *303*, 1352−1355. (b) Koutsopoulos, S.; Kaiser, L.; Eriksson, H. M.; Zhang, S. *Chem. Soc. Rev.* **2012**, *41*, 1721−1728.

(9) (a) Martin, C.; Zhang, Y. *Nat. Rev. Mol. Cell Biol.* **2005**, *6*, 838−849. (b) Hamamoto, R.; Saloura, V.; Nakamura, Y. *Nat. Rev. Cancer* **2015**, *15*, 110−124.

(10) (a) Schweitzer, B.; Kingsmore, S. *Curr. Opin. Biotechnol.* **2001**, *12*, 21−27. (a) Seelig, G.; Soloveichik, D.; Zhang, D. Y.; Winfree, E. *Science* **2006**, *314*, 1585−1588. (b) Lincoln, T. A.; Joyce, G. F. *Science* **2009**, *323*, 1229−1232. (d) Jiang, Y. S.; Li, B.; Milligan, J. N.; Bhadra, S.; Ellington, A. D. *J. Am. Chem. Soc.* **2013**, *135*, 7430−7433.

(11) (a) Cohen, C.; Lohmann, C. M.; Cotsonis, G.; Lawson, D.; Santoianni, R. *Mod. Pathol.* **2003**, *16*, 574−583. (b) Chi, Y.; Wang, X.; Yang, Y.; Zhang, C.; Ertl, H. C.; Zhou, D. *Mol. Ther. Nucleic Acids* **2014**, *3*, e208.

(12) (a) Dubertret, B.; Calame, M.; Libchaber, A. J. *Nat. Biotechnol.* **2001**, *19*, 365−70. (b) Wu, P.; Hwang, K.; Lan, T.; Lu, Y. *J. Am. Chem. Soc.* **2013**, *135*, 5254−5257. (c) Paliwoda, R. E.; Li, F.; Reid, M. S.; Lin, Y.; Le, X. C. *Anal. Chem.* **2014**, *86*, 6138−6143.

(13) Wang, X.; Corin, K.; Baaske, P.; Wienken, C. J.; Jerabek-Willemsen, M.; Duhr, S.; Braun, D.; Zhang, S. *Proc. Natl. Acad. Sci. U.S.A.* **2011**, *108*, 9049−9054.

(14) Hill, H. D.; Millstone, J. E.; Banholzer, M. J.; Mirkin, C. A. *ACS Nano* **2009**, *3*, 418−424.

(15) (a) Arikuma, Y.; Takeda, K.; Morita, T.; Ohmae, M.; Kimura, S. J. *J. Phys. Chem. B* **2009**, *113*, 6256−6266. (b) Guerrero, A. R.; Caballero, L.; Adeva, A.; Melo, F.; Kogan, M. J. *Langmuir* **2010**, *26*, 12026−12032.

(16) Jin, R.; W, G.; Li, Z.; Mirkin, C. A.; Schatz, G. C. *J. Am. Chem. Soc.* **2003**, *125*, 1643−1654.

(17) (a) Anker, J. N.; Hall, W. P.; Lyandres, O.; Shah, N. C.; Zhao, J.; Van Duyne, R. P. *Nat. Mater.* **2008**, *7*, 442−453. (b) Chen, Y.; O'Donoghue, M. B.; Huang, Y. F.; Kang, H.; Phillips, J. A.; Chen, X.; Estevez, M. C.; Yang, C. J.; Tan, W. *J. Am. Chem. Soc.* **2010**, *132*, 16559−16570. (c) Griffin, J.; Singh, A. K.; Senapti, D.; Rhodes, P.; Mitchell, K.; Robinson, B.; Ru, E.; Ray, P. C. *Chem.—Eur. J.* **2009**, *15*, 342−351. (d) Chou, L. Y.; Chan, W. C. *Adv. Healthc. Mater.* **2012**, *1*, 714−721.

(18) http://blast.ncbi.nlm.nih.gov/.

(19) Seferos, D. S.; Giljohann, D. A.; Hill, H. D.; Prigodich, A. E.; Mirkin, C. A. *J. Am. Chem. Soc.* **2007**, *129*, 15477−15479.

(20) Alix-Panabières, C.; Pantel, K. *Nat. Rev. Cancer* **2014**, *14*, 623−631.

DOI: 10.1021/jacs.5b01778
J. Am. Chem. Soc. 2015, 137, 6829−6836

(21) Vigderman, L.; Manna, P.; Zubarev, E. R. *Angew, Chem. Int. Ed.* **2011**, *50*, 636−641.
(22) Seferos, D. S.; Prigodich, A. E.; Giljohann, D. A.; Patel, P. C.; Mirkin, C. A. *Nano, Lett.* **2009**, *9*, 308−311.
(23) Zhou, R.; Zhou, H.; Xiong, B.; He, Y.; Yeung, E. S. *J. Am. Chem. Soc.* **2012**, *124*, 13404−13409.
(24) (a) Grant, B. D.; Donaldson, J. G. *Nat. Rev. Mol. Cell. Biol.* **2009**, *9*, 597−608. (b) Choi, C. H.; Hao, L.; Narayan, S. P.; Auyeung, E.; Mirkin, C. A. *Proc. Natl. Acad. Sci. U.S.A.* **2013**, *110*, 7625−7630.
(25) Pang, H. B.; Braun, G. B.; Friman, T.; Aza-Blanc, P.; Ruidiaz, M. E.; Sugahara, K. N.; Teesalu, T.; Ruoslahti, E. *Nat. Commun.* **2014**, *5*, 4904.
(26) Han, G.; Xing, Z.; Dong, Y.; Zhang, S.; Zhang, X. *Angew, Chem. Int. Ed.* **2011**, *123*, 3524−3527.
(27) (a) Morris, M. C.; Depollier, J.; Mery, J.; Heitz, F.; Divita, G. *Nat. Biotechnol.* **2001**, *19*, 1173−1176. (b) An, M.; Wijesinghe, D.; Andreev, O. A.; Reshetnyak, Y. K.; Engelman, D. M. *Proc. Natl. Acad. Sci. U.S.A.* **2010**, *107*, 20246−20250.
(28) Yamanaka, K.; Nakahara, T.; Yamauchi, T.; Kita, A.; Takeuchi, M.; Kiyonaga, F.; Kaneko, N.; Sasamata, M. *Clin. Cancer Res.* **2011**, *17*, 5423−31.
(29) Peng, X. H.; Cao, Z. H.; Xia, J. T.; Carlson, G. W.; Lewis, M. M.; Wood, W. C.; Yang, L. *Cancer Res.* **2005**, *65*, 1909−1917.

DOI: 10.1021/jacs.5b01778
J. Am. Chem. Soc. 2015, 137, 6829−6836